Inclusive inelastic scattering of 96.5-MeV π^+ and π^- by the hydrogen and helium isotopes

M. A. Khandaker,* M. Doss,† I. Halpern, T. Murakami,‡ D. W. Storm, and D. R. Tieger§
University of Washington, Department of Physics, FM-15, Seattle, Washington 98195

W. J. Burger**
Massachusetts Institute of Technology, Bates Linear Accelerator Center, Middleton, Massachusetts 01949
(Received 24 May 1990)

Spectra, angular distributions, and integrated cross sections for inclusive inelastic scattering of 96.5-MeV π^+ and π^- from ^{2}H, ^{3}He, and ^{4}He are presented. The measurements were made using a high-pressure gas cell, which permits an accurate determination of relative cross sections for all targets. The data are compared with distorted-wave impulse-approximation calculations and with a modified plane-wave impulse-approximation calculation. In addition, by combining the total inelastic cross sections from this work with estimates of single-charge-exchange cross sections and with published values and reasonable estimates of the other π^+ cross sections at the same energy, values for total reaction and pion absorption cross sections are obtained for all the targets. The dependence of these cross sections on Z, N, nuclear density, and nuclear binding energy is discussed in terms of a simple model.

I. INTRODUCTION

The interactions of medium-energy pions with nuclei are dominated by three processes: elastic scattering, true absorption, and inelastic scattering to the continuum. Studies of inclusive inelastic scattering at energies up to that of the delta resonance [1–5] indicate that this process predominantly involves the interaction of the pion with just one nucleon in the nucleus. Simple models [6, 7] based on this assumption give a reasonable account of many features of the interaction of medium-energy pions with heavy nuclei.

The assumption of a single interaction should be even more valid for the very lightest nuclei — the hydrogen and helium isotopes. Moreover, this small group of nuclei provides considerable variations of nuclear densities, ratios of protons to neutrons, and nucleon binding energies. This makes them more suitable than heavy nuclei for studying the dependence of the pion's interactions in nuclei on these important parameters. Inclusive scattering of 100-MeV π^+ [4, 5] and of 90- and 120-MeV π^+ and 120-MeV π^- [1] has been measured on ^{4}He. Additionally, π^+ and π^- scattering from ^{3}He have been studied at 170 MeV and higher incident energies [3]. The interactions of pions with the helium isotopes have been reviewed in detail [8].

In spite of the variety of available data, it has not been possible to compare inclusive inelastic scattering from the helium and hydrogen isotopes with sufficient accuracy to identify clearly the dependence of the pion interactions on the nuclear parameters mentioned above. Furthermore, the effect of the nuclear features on the ratio of total inelastic scattering to pion absorption is important, because absorption is the strongest channel competing with inelastic scattering. There are data for particular absorption modes [5, 9–16], but the total absorption cross sections, except [17] for ^{2}H, are not well known.

We have measured the inclusive inelastic (and elastic) scattering of 96.5-MeV π^+ and π^- from ^{2}H, ^{3}He, and ^{4}He. This incident energy (nominally 100 MeV) was chosen because we have had success using simple classical models to describe our previous 100-MeV results with heavier nuclei [6], and we wanted to extend that work to light nuclei.

A high-pressure gas cell was used for the targets. It permitted a more precise and direct comparison of the relative scattering cross sections for the different targets than is otherwise possible. An accurate comparison of cross sections is necessary in order to be able to separate the influence of true absorption and elastic-scattering from inelastic-scattering processes. The experimental details are given in Sec. II.

In Sec. III, we present measured elastic and inclusive inelastic differential cross sections and spectra. We also attempt, using available published results or model estimates, to obtain values for charge-exchange and true absorption cross sections. These cross sections, in particular the true absorption cross sections, are needed for any comprehensive account of the interaction of pions in these nuclei.

In Sec. IV, we compare the resulting differential and total inelastic cross sections with various models, including distorted-wave impulse-approximation (DWIA) calculations of inclusive spectra. We find that the inclusive scattering results are well described in terms of single pion-nucleon scattering, although, at the most for-

ward angle (40°) we observe significantly fewer pions than are predicted by the DWIA. We show how the magnitudes of the inelastic-scattering cross sections are intimately related to the amount of absorption, and we use a plane-wave impulse-approximation (PWIA) calculation, corrected for absorption, to separate inelastic quasifree scattering from that part which is elastic. In addition we examine, in terms of a simple classical model, how the true absorption cross section can be related to the free π-nucleon cross section, the number of $T = 0$ nucleon pairs, and the mean nuclear density.

II. EXPERIMENTAL PROCEDURE

The experiment was carried out on the M11 pion channel [18, 19] at the Tri-University Meson Facility (TRIUMF). The general arrangement of the detection apparatus is shown in Fig. 1. We used a high pressure gas target with the QQD spectrometer, which has a broad (25%) [20,21] momentum acceptance and a large (22 msr) solid angle. Spectra of scattered pions were obtained at 40°, 60°, 75°, 100°, and 125° with respect to the beam. Details of the experiment are contained in Ref. [22].

A. Beam description

The channel momentum acceptance $\Delta P/P$ (FWHM) was typically set at 1.5%. With a peak proton beam current between 100 and 120 μA, average fluxes of 100-MeV pions at the target location were 2×10^6 π^+/s or 1×10^6 π^-/s. The incident pion flux was determined using two plastic counters, $BM1$ and $BM2$, located directly in the beam upstream from the target. Counter $BM2$ had a 30-mm-diameter hole and was used as a veto to define the effective size of the beam incident on the target cylinder.

B. Targets

The primary targets studied were ^{2}H, ^{3}He, and ^{4}He. At each angle we also collected data for pions scattered from ^{1}H in order to normalize the results for the other targets to the known π–proton cross sections [23]. To permit a direct and precise comparison of the relative yields of the scattered pions, we chose to use a high-pressure (100 atm) gas target. The gas density was determined to an accuracy of better than 1%; such precision has not even been approached with liquid ^{3}He to our knowledge. Thus the ratio of cross sections between one target and another can be determined with the high accuracy which is required for our comparisons.

In designing the target vessel, the target geometry and wall thicknesses were carefully considered. A 41-mm-radius cylinder of 350 mm length, with hemispherical end caps, suited both the acceptance of the spectrometer and the size of the beam. A high strength aluminum alloy was chosen to minimize multiple scattering. The hemispherical cap was 3.2 mm thick while the cylinder wall was 6.4 mm thick. With these dimensions, the stress on the target vessel was 1/8 of the yield stress at 100 atm pressure, and multiple scattering was not a serious problem. Data from empty-target runs showed that the target walls contributed less than 2% of the total counts in the inelastic spectrum from a filled target.

At a nominal operating pressure of 100 atmospheres and at room temperature the target "thicknesses" that were used for the different gases were the following: ^{1}H, 55 mg/cm^2; ^{2}H, 115 mg/cm^2; ^{3}He, 85.9 mg/cm^2; and ^{4}He, 115 mg/cm^2. These thicknesses corresponded to a length of 70 mm at the center of the cylinder, matching the acceptance of the spectrometer.

The 100-MeV incident pions lost 2.2 MeV on their way into the cylinder. Due to the additional energy loss in the gas, the average energy of the pion beam interacting with the various gases at the center of the target was 96.5 MeV. As the pions left the container they did not lose more than 5 MeV, on the average, for our most forward (40°) or backward (125°) angles.

C. The magnetic spectrometer and wire chambers

The physical layout of the spectrometer and wire chambers used in this experiment is shown in Fig. 1. This system has been described earlier in detail [20, 21]. The overall momentum resolution that was measured during the data collection period was $\Delta P/P \approx 1.7\%$, with most of this spread resulting from the channel setting. This resolution is completely satisfactory for a continuum measurement like this one.

In order to measure continuum spectra, it is important to obtain an accurate measurement of the relative efficiency of the spectrometer as a function of δ, the fractional shift from P_0, the nominal central momentum of the spectrometer. This was done by stepping the peak from a hydrogen target across the focal plane, varying the field while sitting at a fixed angle (100°) and beam energy. Checks were made to ensure that the relative efficiency was not dependent on the field setting. The resulting relative efficiency is presented in Fig. 2. The data for the pion spectra and for the efficiency measurements were subjected to identical cuts. We used the spectrometer acceptance from $\delta = -12.5\%$ to $\delta = +12.5\%$. Four

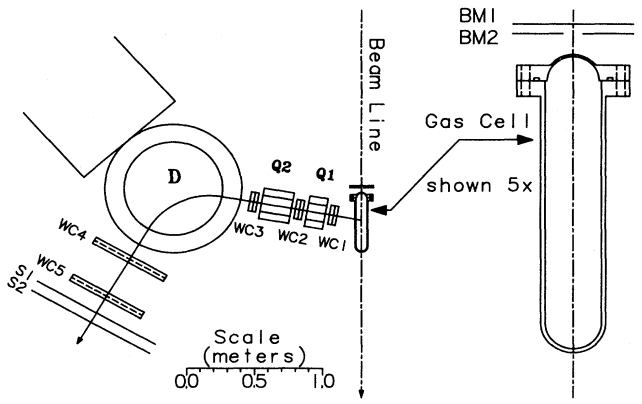

FIG. 1. Layout of the gas cell and QQD spectrometer.

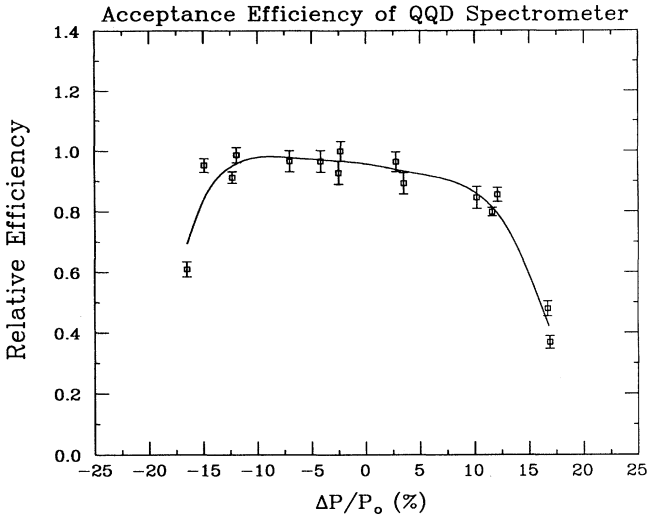

FIG. 2. Relative acceptance efficiency of the QQD spectrometer. The solid curve is a cubic-spline fit to the measurements.

magnet settings were used for most of the spectra, allowing measurement of pions from 24 to 100 MeV and providing sufficient overlap of momentum bites. Relative decay corrections were applied to the pion spectra, to account for the energy dependence of the pion decay length.

D. Particle identification

The beam from the channel contained pions, muons, electrons, and, when using positive pions, also protons. Protons were removed from the pion beam by degrading their momenta with a foil placed halfway down the channel. The pions, muons, and electrons were separated by a time-of-flight (TOF) technique, timing against a pickup driven by the proton beam. The relative intensity ratios of π:μ:e were typically 1000:41:23 for a π^+ beam and 1000:37:33 for a π^- beam.

E. Data obtained — Cuts

Each event contained scintillation counter pulse heights, times of flight, and wire chamber information. We only kept events with one hit in each wire plane. Typical chamber efficiencies were above 99% for the back chambers and were between 92 and 96% for $WC3$. Because of high singles rates in $WC1$, its efficiency varied from 77 to 93 %.

We chose a target fiducial phase space 70 mm long (along the beam direction), 120 mr horizontal, 28 mm high, and 200 mr vertical. Trajectories originating outside of this region or falling outside a fiducial area of $WC1$ were excluded. The bend plane information from both front chambers and from only one of the back chambers was needed to determine the momentum, and the vertical coordinates in the two front chambers could be used to predict the vertical position in the back chambers. Thus there were three redundant coordinates for each trajectory. Trajectories were discarded when either scattering in the spectrometer or pion decay to a muon were identified by the inconsistency of the wire chamber coordinates.

The events surviving the cuts were histogrammed according to δ, and the corrections for relative efficiency and pion decay were applied. Finally, the results from the various spectrometer settings were combined to produce the final energy spectra, shown in Fig. 3.

F. Uncertainties

Since this experiment involves a comparison of pion scattering from several gases used sequentially in the same container, a number of experimental uncertainties cancel in the determination of relative cross sections. For positive pions, sufficient data were collected to give an average statistical uncertainty of less than 5% per MeV bin size in the peak region of the continuum spectrum for each target. For negative pions this statistical accuracy was only about 10%. The remaining systematic uncertainties are estimated and presented in Table I. Finally, the values of all of our measured cross sections include a common 5.5% normalization uncertainty resulting from the uncertainty in the π-p cross sections [23].

III. MEASURED AND INFERRED CROSS SECTIONS

A. Cross sections measured in the present experiment

The immediate results of this experiment consist of spectra (Fig. 3) of pions scattered from ^{2}H, ^{3}He, and ^{4}He measured at several angles. The elastic yields at each angle were extracted by fitting a line shape obtained from the measured π^+-p scattering. To obtain the energy-integrated inelastic differential cross sections it was necessary to extrapolate the cross sections at the low end of the spectra below the low-energy cutoff. The fraction of the total extrapolated contribution to the integral was very small in any reasonable extrapolation. The estimated contribution to the uncertainty in the differential cross section was never greater than 3%. The elastic and inelastic differential cross sections that we obtained are in good agreement with earlier measurements at similar pion energies [1, 4, 24]. They are plotted in Figs. 4 – 6.

Our measurements covered the limited angular range from 40° to 125°. At angles forward of 40° the tail of the growing elastic line makes the extraction of the inelastic spectrum increasingly uncertain, and the singles rate in $WC1$ increases rapidly. The spectrometer could not be moved to angles beyond 125°. It was therefore necessary to extrapolate the differential cross sections to 0° and to 180° in order to obtain the total inelastic cross section. For the π^+ data, this extrapolation was done by fitting to a quadratic in $\cos(\theta)$. As has been observed in heavier

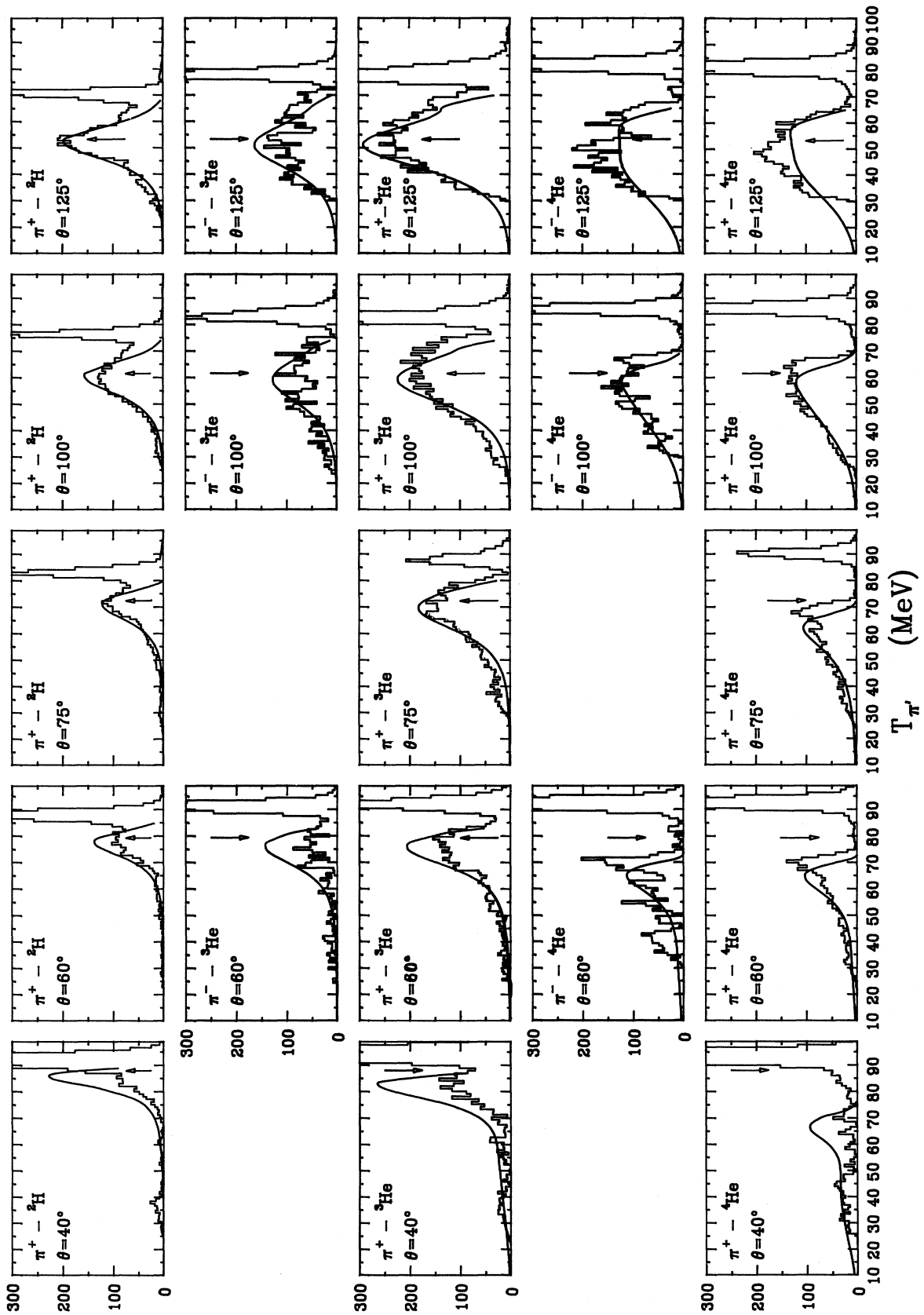

FIG. 3. Inclusive spectra of scattered pions from ^{2}H, ^{3}He, and ^{4}He. The histograms are the measurements, the solid curves are the DWIA calculations of inclusive inelastic scattering, and the arrows indicate the kinetic energy of a pion scattered by a free proton.

TABLE I. Uncertainties in the energy-integrated cross sections (%).

Relative efficiency[a]	2–3
Background from target vessel	<2
Target thickness	<1
Matching different momentum bites	<2
Subtraction of tail of elastic peak	
Back angles	0.2
Forward angles	3–4
Typical statistical uncertainties[b]	
Chamber efficiencies	0.3
Counting statistics (integrated spectrum)	1.7

[a] Spectra of different shapes emphasize different parts of the relative acceptance efficiency of the spectrometer. Consequently, uncertainties in this function do not cancel completely in the normalization to ^{1}H.

[b] The statistical uncertainties varied from spectrum to spectrum.

nuclei [6], the angular distributions vary slowly enough with angle that no higher powers than $\cos^2(\theta)$ seem necessary. We obtained π^- data on the helium isotopes at only three angles, 60°, 100°, and 125°, and the statistics are not as good as for the π^+ measurements. The π^--^{4}He results match the π^+ results, as expected. The three data points for π^--^{3}He fit well to a linear function of $\cos(\theta)$, so for this case we used this form for the angular extrapolation. The smoothness of the angular distribution and the fact that the cross section drops off at forward angles limit the uncertainties due to extrapolations in angle. In the worst case, π^- on ^{3}He, we estimate a 12% uncertainty in the total cross section due to this extrapolation.

Our measured inclusive inelastic-scattering cross sections for π^+ on ^{2}H and ^{4}He and for π^+ and π^- on ^{3}He are listed in Table II. Since π^+ and π^- cross sections for ^{4}He are identical within the accuracy of our measurements, we can consider the π^- on ^{3}He cross sections to represent those for π^+ on ^{3}H at the same energy. Thus we effectively have the inelastic π^+ cross sections for the four nuclei ^{2}H, ^{3}H, ^{3}He, and ^{4}He.

We also list in Table II the total elastic-scattering cross sections (i.e., the angle-integrated nuclear parts of the elastic-scattering cross sections). These were obtained from optical model fits (see Sec. IV) to our data, and, for the case of π^- on ^{3}He, to additional data [24] as well.

B. Relevant cross sections obtained from earlier measurements or from estimates

To help interpret inclusive inelastic and elastic scattering in the context of a consistent picture of the pion–nucleus interaction, charge-exchange and total absorption cross sections are important. Along with our results, we list in Table II the cross sections measured (by others) or inferred for these other types of pion interactions with the hydrogen and helium isotopes at the energy of our experiment. The determination of these cross sections is described in the following.

1. Charge-exchange cross sections

Because the inclusive single-charge-exchange (SCX) cross sections have not been measured for these targets in our energy range, we estimate them from the inelastic cross sections, using N, Z, and the ratios of the free pion-nucleon scattering and charge-exchange cross sections. This type of estimate for SCX cross sections gives reasonable agreement with measured data [25] at 142 MeV for π^- on ^{2}H, where the prediction of 22.5 mb compares with the measured 26.5 ± 3 mb. Also for 100-MeV π^+ SCX reactions on ^{16}O an estimate [2] of 55 ± 5 mb compares well with the measured [26] 66 ± 10 mb. We estimate a 15% uncertainty in the single-charge-exchange cross sections obtained in this way.

We note that the double-charge-exchange cross section for ^{4}He at 120-MeV incident pion energy [27, 28] is 128 μb, which is negligible compared to the estimate for the SCX cross section. We therefore ignore the contribution of double-charge-exchange to the total reaction cross section for all the targets.

2. True absorption cross sections

True absorption cross sections have been measured [17] for 95-MeV pions incident on ^{2}H. Although the true absorption cross section has not been measured for the helium isotopes in the region of 100 MeV, differential cross sections have been obtained in kinematically complete measurements of ^{3}He pion absorption over a reasonable range of angles at a number of energies. We estimate the total π^+ absorption cross section in ^{3}He by first estimating the size of the two-nucleon absorption cross section and then estimating the ratio of the total absorption to the two nucleon absorption. Values obtained for the ratio of the cross section for two-body absorption in ^{3}He to the ^{2}H(π^+, pp) cross section vary from 1.52 ± 0.15 (at 82.5 MeV) [12] to 2.2 (at 120 MeV, obtained, however, in a single arm experiment at a single angle) [10]. At lower energies, values of 1.36 ± 0.14 (at 62.5 MeV) [12] and of 1.44 ± 0.30 (at 65 MeV) [11] have been reported. It seems reasonable to assume that the cross section for two-body absorption in ^{3}He at 96.5 MeV is 1.6 ± 0.3 times the ^{2}H(π^+, pp) cross section.

Furthermore, the ratio of three-body absorption to two-body absorption for π^+ on ^{3}He has been estimated to be 0.42 ± 0.17 at 82.5 MeV [12] or 0.25 at 120 MeV[13]. These estimates are based on samples of the double-differential cross section for angle pairs for which the undetected nucleon must receive significant momentum transfer. We will take the π^+ true absorption cross section on ^{3}He to be 1.6 times 1.3 times that on the deuteron. Including the uncertainties, this factor is 2.1 ± 0.4, giving an estimated total absorption cross section of 20 ± 4 mb for π^+ on ^{3}He.

For π^- on ^{3}He two neutrons are the outgoing products from the absorption on a $T = 0, S = 1$ nucleon pair. Consequently, this absorption channel is difficult to study, and absorption cross section results are not available.

For the case of pion absorption on ^{4}He, two-particle [15] and three-particle [16] coincidence measurements

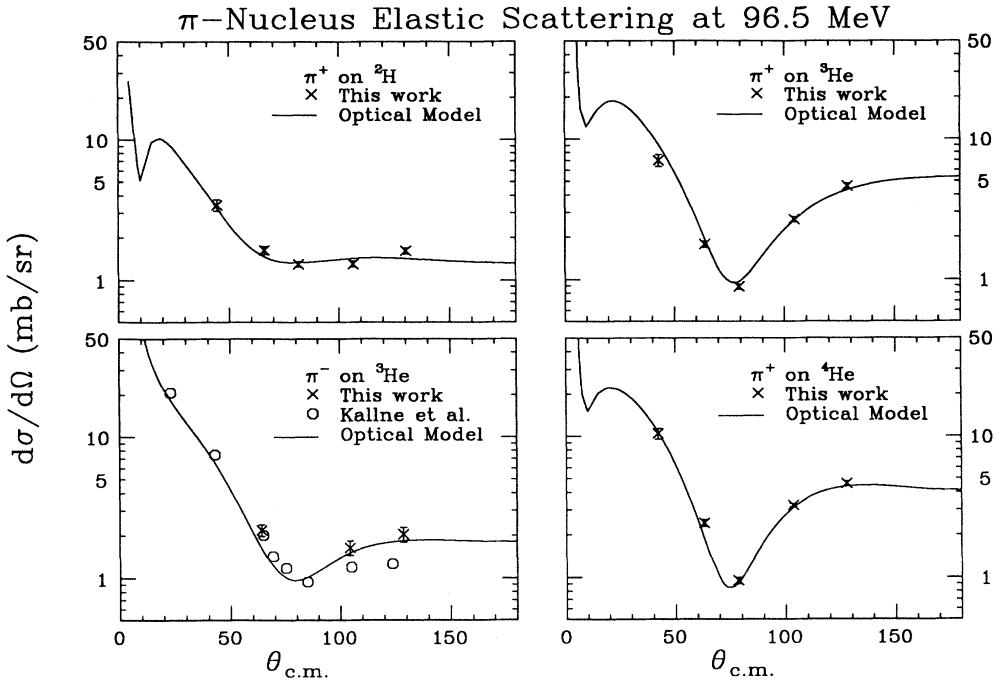

FIG. 4. Angular distributions of elastic pion scattering. The solid curves result from the optical model calculations described in the text.

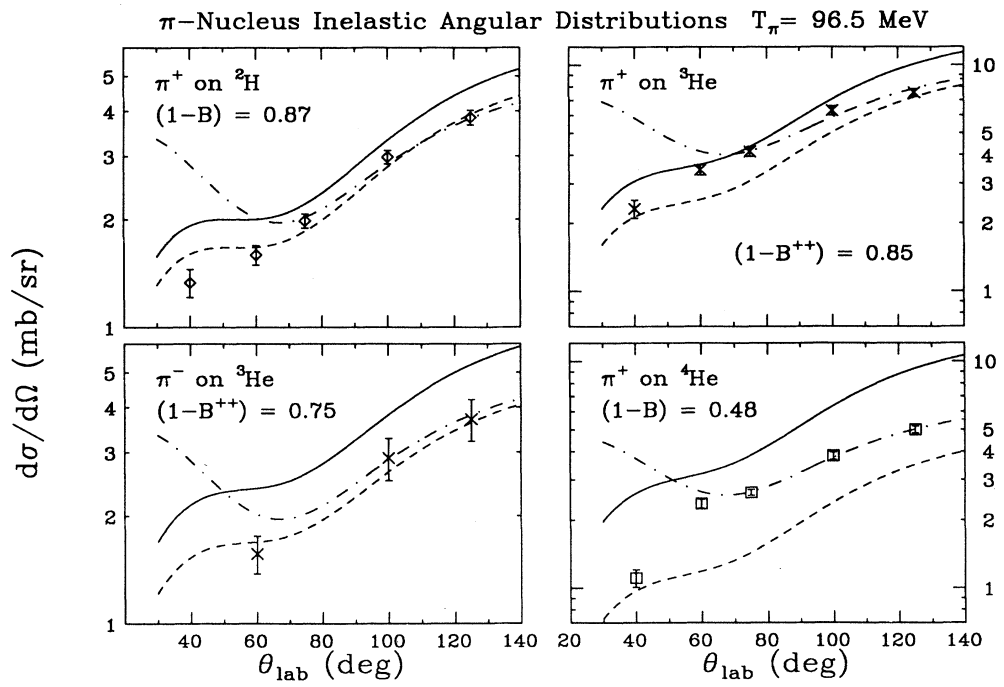

FIG. 5. Angular distributions of inclusive inelastic pion scattering. The solid curves are the PWIA calculation given by Eq. (4). The dashed curves are the PWIA calculations modified by shadowing and by factors $(1 - B^{++})$ and $(1 - B^{+})$, as described by Eq. (5). The dash-dot curves are the free π^+-proton scattering differential cross section, times the empirical factor R described in the text.

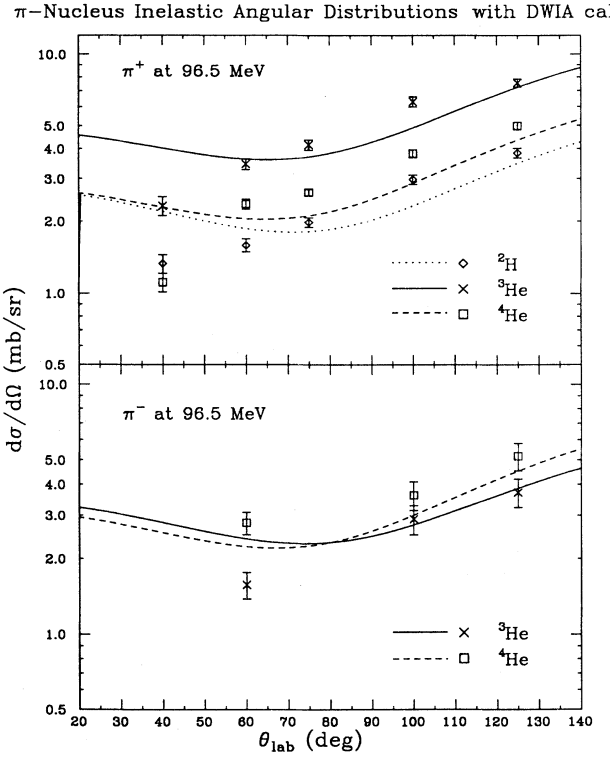

FIG. 6. Angular distributions of inclusive inelastic pion scattering. The curves result from the DWIA calculations described in the text.

have been made at various angle pairs in order to attempt to understand the relative amounts of two-, three-, and four-nucleon absorption processes. Cloud, bubble, and streamer chamber measurements [29–32] have also been reported, but the results are in strong disagreement. More accessible for our purposes are the total cross-section measurements [33,34] (using transmission techniques) for both π^+ and π^- for pion energies around 100 MeV. Interpolating the results of those authors to 96.5 MeV, we find for π^+ [33] a value of 178 ± 6 mb, while for π^- the values are 199 ± 6 (Ref. 33) or 200 ± 2 (Ref. 34). These results have been Coulomb corrected, but Johnson [33] points out that averaging the results for both pion charges will reduce remaining ambiguities in the Coulomb correction. Thus we use a value of 189 ± 6 mb for the total cross section. Subtracting the elastic, inelastic, and estimated single-charge-exchange cross sections gives an absorption cross section of 63 ± 10 mb for π^+ on ^{4}He. This value can be compared with an interpolation of values given in Ref. 1 which yields about 76 mb. This value is higher than our estimate, primarily because those authors used only the 200 mb total cross section of Ref. 34.

With these values for the absorption cross section combined with our measurements of the total inelastic scattering and our estimates of the total charge-exchange cross section, we can also obtain the total reaction cross section, which we will use in Sec. IV to test optical model parameters. In Table II we list all of the cross sections obtained as explained above.

IV. DISCUSSION

We begin this section with summaries of the general features of the inclusive inelastic-scattering and of the absorption cross sections that we have deduced in the previous section. These two reaction channels, along with elastic scattering, account for virtually all of the pion interactions with the very light nuclei of this experiment. We will try to understand the observed features of all three of these channels consistently in terms of relevant nuclear properties.

In the following sections we will describe three different calculations that we have undertaken in order to stress different ideas. The first calculation is based on a simple classical description of the pion-nucleus interaction. It connects the relative amounts of scattering and true absorption with the properties of the initial interaction between the pion and one nucleon in the nucleus. The second calculation uses the PWIA which allows us to separate elastic and inclusive inelastic scattering. By combining the absorption picture used in the classical model with the PWIA, we are able to include the effects of pion flux removal as the pion penetrates the nucleus. These

TABLE II. Measured and inferred integrated cross sections (mb) for pion interactions in hydrogen and helium isotopes at 96.5 MeV. Estimated cross sections are enclosed in parentheses. For each target either the absorption or total reaction cross section is obtained algebraically from the others. The cross section so obtained is enclosed in square brackets.

	π^+-p	π^+-n	π^+-^{2}H	π^+-^{3}He	π^--^{3}He	π^+-^{4}He
Elastic cross section	55.5[a]	5.8[a]	31.3±3.2	66.6±6.7	40.0±6.0[c]	72.8±7.3
Inelastic			34.1±1.7	67.3±3.2	32.0±4.3	42.1±1.5
Absorption			9.6±0.2[b]	(20±4)		[63±10]
SCX		16.4[a]	(9.1±1.4)	(9.5±1.4)	(15.5±3.1)	(11.3±1.7)
Total reaction			[53±3]	[97±6]		116.±9[d]

[a] See Ref. 23.
[b] See Ref. 17.
[c] See Ref. 24.
[d] Average of results for π^+ and π^- from Ref. [33] and Ref. [34].

two calculations taken together provide a consistent and explicit, although clearly oversimplified, picture of the interplay between pion absorption, elastic scattering, and inelastic scattering in a quasifree model.

The last of the three calculations uses the DWIA. It is our most complete calculation, in the sense that the wave functions of the interacting pions and nucleons are well described and the elementary interactions are treated reasonably. However, true absorption of pions is included in the DWIA in an indirect manner, via the imaginary part of the π-nucleus optical potential. For that reason the classical model and the PWIA calculations are valuable aids for understanding the absorption mechanism and for understanding the interplay between "quasifree" scattering and true pion absorption.

A. General observations

At sufficiently large angles, the observed locations and widths of the peaks of the inelastic-scattering spectra support a quasielastic picture. The peak from ^{2}H is much narrower than the others, as expected, since only in deuterium is the rms nucleon momentum significantly less than that of the incident pion.

The angular distributions for inelastic scattering from all three targets exhibit little structure, no minimum, and are backward peaked. Furthermore, for angles greater than or equal to 75°, all the angular distributions have shapes very similar to that for free π^+-proton scattering, as shown in Fig. 5. Values of R, the ratio of the inelastic differential cross section to that for elastic scattering on a proton at angles beyond 75°, are given in Table III.

Qualitatively, one can understand some of the relative values of the R's by considering a quasifree picture for inelastic scattering, in the presence of competition with the other major channels. Thus the cross section for inelastic scattering from ^{2}H is expected to be less than the cross section for scattering from a proton, because in ^{2}H the neutron contributes negligibly to the scattering of π^+ at the angles of this experiment, and there is competition with both the elastic channel and true absorption of the pion. The π^+ inelastic scattering from ^{3}He is about twice as large as it is from ^{2}H or from π^- on ^{3}He, as might be expected from the dominance of π^+-proton over π^+-neutron interactions. The π^+ cross section in ^{4}He is substantially less than twice that in ^{2}H, presumably because of the greatly increased absorption in ^{4}He (see Table II) and the suppression resulting from the high threshold for inelastic scattering. As expected from charge symmetry, the π^+ and π^- scattering cross sections on ^{4}He are the same.

Finally, we consider the absorption cross sections, which are observed to increase by a factor of 6 between ^{2}H and ^{4}He. The dramatic increase in the density of these nuclei with increasing A can be expected to have an impact on the absorption cross section. Also, one expects [9, 12] that for these s-shell nuclei the two-body absorption will take place primarily on pairs of nucleons initially coupled to $T = 0$, and the number of such pairs increases by a factor of 3 between ^{2}H and ^{4}He.

B. Classical model

The nuclei under consideration are simple systems, and since the correspondence principle should apply in the continuum well above threshold, a classical treatment is appropriate. Consequently, we have developed a model which relates both the scattering and the relative absorption cross sections to known free scattering cross sections, nuclear densities and isospin, and to an empirical parameter B, the fraction of interacting pions which are absorbed. We will examine whether B varies with the density and isospin of the nuclei studied in a reasonable and predictable manner. Additionally, we will be able to use B in another simple calculation, the modified PWIA, below.

There are Monte Carlo intranuclear cascade calculations reported in the literature which have been used to calculate inelastic and absorption cross sections in the same spirit [35, 36]. Such calculations have the apparent advantage of treating major physical effects precisely in a properly defined geometry. However, the results, particularly for 100-MeV pions [36], seem to depend strongly upon quantities, such as the mean free path of the Δ, which are neither well known nor of specific relevance to the present discussion. Furthermore, it is difficult to evaluate the relative importance of different physical processes. Often simpler calculations [6, 7, 37] can provide insight and can test the extent to which a few basic physical ideas are sufficient to explain most of the observed phenomena.

Specifically, we assume that in the nucleus the cross section for an incident pion to combine with a nucleon is equal to the free scattering (including charge exchange) cross section, times a factor for the reduction of pion flux at the site of the chosen nucleon, due to the other nucleons in the nucleus. This shadowing is characterized by Z_e and N_e, the effective numbers of nucleons available to interact with an incident pion, as calculated [22] using known nucleon density distributions and free π-nucleon cross sections [23]. Values are given, for π^+ incident, in Table IV.

We assume that if an interacting pion-nucleon complex decays, the pion will emerge from the nucleus without any further interaction. This assumption is reasonable, because of the small number of nucleons in these

TABLE III. Average ratio, R, of inelastic differential cross sections to the elastic cross section for π^+-p scattering at angles $\geq 75°$.

	π^+-^{2}H	π^+-^{3}He	π^--^{3}He	π^+-^{4}He	π^--^{4}He
R	0.71 ± 0.02	1.44 ± 0.04	0.70 ± 0.07	0.92 ± 0.02	0.92 ± 0.08

TABLE IV. Effect of Shadowing.

	Z_e/Z	N_e/N
^{2}H	0.965	0.915
^{3}H	0.915	0.865
^{3}He	0.865	0.828
^{4}He	0.785	0.738

targets. Empirically, this assumption is supported by the observed spectrum shapes, the angular distributions, and the negligibly small cross-section for double-charge-exchange scattering [27, 28] from ^{4}He. In a fraction B of the initial interacting complexes the pion is absorbed before decay takes place.

In this picture, the absorption cross section for π^+ can be written as

$$\sigma^{\rm abs} = Z_e\sigma^{++}(B^{++}) + N_e\sigma^{+}(B^{+}) \ , \qquad (1)$$

where

$$\sigma^{++} \equiv \sigma[(\pi^+ + p) \rightarrow (\pi^+ + p)] = 55.5 \text{ mb}$$

and

$$\sigma^{+} \equiv \sigma[(\pi^+ + n) \rightarrow (\pi^+ + n) \text{ or } (\pi^0 + p)] = 22.2 \text{ mb}.$$

The value of B for the π^+-proton complex, B^{++}, may differ from the value for the π^+-neutron complex, B^+.

In order to relate the B values that are obtained from the data to the properties of the nuclei, we express B in terms of the ratio of an absorption width W_a to a decay width W_d:

$$B = \frac{W_a}{W_d + W_a} = \frac{\gamma}{1+\gamma},$$

where

$$\gamma = W_a/W_d.$$

Here W_d is assumed independent of the nucleus while W_a is taken to vary from nucleus to nucleus. For a given nucleus B^+ and B^{++} are simply related. For ^{3}He, for example, there are twice as many possible absorbing partners for the π^+-n complex (which needs a proton) as for the π^+-p complex. Hence, for ^{3}He, $W_a^+ = 2W_a^{++}$. In general, one can write $NW_a^+ = ZW_a^{++}$ for all of the nuclei of this experiment. With this relation and with Eq. (1), values for γ^{++} can be estimated for each target from its measured absorption cross section. Then one can see whether the extracted values of γ^{++} are proportional to the density of neutrons that coupled to $T = 0$ with the proton involved in the initial interaction.

It is possible to get an independent estimate of the γ^{++} values from inelastic-scattering cross sections. If one ignores the contribution of the decaying systems to elastic scattering, one can write an equation for inelastic scattering that is complementary to Eq. (1), namely,

$$\frac{d\sigma_{\rm inel}}{d\Omega} = Z_e(1 - B^{++})\frac{d\sigma_p}{d\Omega} + N_e(1 - B^{+})\frac{d\sigma_n}{d\Omega}. \qquad (2)$$

Since it is more reasonable to ignore elastic scattering at backward than at forward angles, we obtain values for γ from the differential cross sections for angles of 75° and greater. Because of the (unknown amount of) competition from elastic channels, the B and corresponding γ values obtained using Eq. (2) should be regarded as upper limits.

Along with the B^{++} values deduced from absorption cross sections, we list upper limits deduced from the inclusive inelastic-scattering differential cross sections in Table V. The two sets of values are seen to be consistent. In comparing the γ^{++} values for different nuclei we use those obtained from the absorption measurements, except for the case of π^+ on ^{3}H, where such measurements are not available. Here we use the value obtained from inelastic scattering (actually that of π^- on ^{3}He). The good match between B's calculated from scattering and absorption cross sections for ^{3}He lends credibility to the use of scattering data for this assignment in ^{3}H.

To understand the systematic behavior of the extracted γ^{++} values, we must take into account the numbers of nucleons that can lead to absorption in the different nuclei. Since the range of the interaction leading to pion absorption is short, we expect that γ^{++} should be proportional to the mean density of neutrons available to

TABLE V. Deduced branching ratios and ratios of widths for true pion absorption and decay from π^+-p complexes. Ratios are obtained using B^{++} from $\sigma^{\rm abs}$ except for the ^{3}H case, as described in the text.

	^{2}H	^{3}H	^{3}He	^{4}He
B^{++} from $\sigma^{\rm abs}$	0.130±0.003		0.15±0.03	0.53±0.08
B^{++} from $d\sigma/d\Omega$ [a]	0.26 ±0.02	0.25±0.08	0.17±0.02	0.41±0.01
γ^{++}	0.149±0.004	0.33±0.14	0.19±0.04	1.1 ±0.3
P ($T = 0$ pairs per proton)	1.00	1.50	0.75	1.50
γ^{++}/P [b]	0.149±0.004	0.22±0.09	0.25±0.05	0.75±0.20
$R_{\rm rms}$ (Fermi)	1.92	1.68	1.68	1.41
$\gamma^{++}/(P/R^3_{\rm rms})$ [c]	1.06 ±0.03	1.04±0.45	1.20±0.20	2.1 ±0.6

[a] Upper limit, as explained in the text.

[b] This row should exhibit constant values if the interaction range leading to absorption is long.

[c] This row should exhibit constant values if the interaction range leading to absorption is short.

form a $T = 0$ pair with the proton of a π^+-p complex. This density is proportional to P, the total number of $T = 0$ pairs divided by Z and by the cube of the nuclear rms radius $R_{\rm rms}$. Both P and this relative density are listed in Table V, and it is seen that for all the targets but ^{4}He, γ^{++} is proportional to this density. The anomalous suppression of inelastic scattering relative to absorption in ^{4}He can also be inferred from the double-charge-exchange data of Gram *et al.* [7]. The large value of γ in ^{4}He may arise from a number of factors. For example, W_d may be smaller for ^{4}He than for the other nuclei because the large binding energy will block those decays which fail to transfer enough energy to the nucleon. Another possibility is that due to the high nucleon density in ^{4}He, W_a may be receiving some additional contribution from many-nucleon absorption mechanisms [14] which bypass the requirement for an initial $T = 0$ pair.

C. Plane-wave impulse approximation

Because these are small nuclei, and because the momentum transfer at forward angles is not large, one expects that a substantial amount of the quasifree scattering at forward angles will produce elastic scattering rather than inelastic. This suppression of the inelastic scattering is described by the PWIA. Ignoring nucleon-nucleon correlations, one can write [38]

$$\frac{d\sigma_{\rm el}}{d\Omega} = |f_p(\theta)Z + f_n(\theta)N|^2|F(q)|^2 \quad (3)$$

and

$$\frac{d\sigma_{\rm inel}}{d\Omega} = [|f_p(\theta)|^2Z + |f_n(\theta)|^2N][1 - |F(q)|^2], \quad (4)$$

where $F(q)$ is the nuclear matter form factor as a function of the momentum transfer q, and $f_p(\theta)$ or $f_n(\theta)$ is the scattering amplitude at the angle θ for pions on protons or on neutrons.

From these equations we can see that a fraction $|F(q)|^2$ of the elementary scattering cross section is removed from the inelastic channels. The corresponding amplitude appears coherently in the elastic channel.

Since we have estimated the effects on the pion flux at the struck nucleon due to shadowing by other nucleons, and also have determined $(1 - B)$, the fraction of π-nucleon interactions that lead to a scattered pion, it is appropriate to include these quantities in Eq. (4), which then becomes (for incident π^+)

$$\frac{d\sigma_{\rm inel}}{d\Omega} = \left(\frac{d\sigma_p}{d\Omega}(1 - B^{++})Z_e + \frac{d\sigma_n}{d\Omega}(1 - B^{+})N_e\right) \times[1 - |F(q)|^2]. \quad (5)$$

To obtain $F(q)$, Gaussian wave functions were used for the helium isotopes and the Hulthen wave function was used for deuterium. For examples of the magnitudes of the form factors, we note that they drop to a value of 0.5 at angles between 40° and 65° depending on the target.

The inclusive inelastic differential cross sections obtained from Eqs. (4) and (5) are shown along with the measured data in Fig. 5. We note that the *elastic* differential cross section, when shadowing and true absorption are significant, must also include diffractive effects which would make it unreasonable to expect Eq. (3) to reproduce even just the shape of the elastic angular distribution. Diffraction effects due to absorption of flux are not present in the inclusive *inelastic scattering*.

When absorption is not included in the PWIA calculation, the predictions are larger than the measured data, although for ^{3}He the predictions are close. The shape of the inelastic angular distributions for angles greater than 75° is reproduced fairly well by the calculation. At forward angles, the calculation indicates that part of the drop in inelastic cross section (compared to π-nucleon scattering) results from the large value of $F(q)$. Including competition from absorption and shadowing gives a good match to the ^{2}H data, but predicts cross sections that are too small for the ^{4}He case. If the value for B^{++} that we have obtained from the absorption cross section are too large, it would account for this discrepancy. Otherwise we have no explanation for it.

D. Distorted-wave impulse approximation

The goal of our discussion so far has been to see how much of the observed phenomena can be explained with the simplest models. On the other hand, a comparison with a calculation which includes all the standard physics is appropriate. To that end, we have performed calculations for the single nucleon knock-out reactions $A(\pi^\pm, \pi^\pm$ p$)B$ and $A(\pi^\pm, \pi^\pm$ n$)B$ in the factorized DWIA [39–41] using the code THREEDEE of Chant [42]. The objective of the calculations was to include distortion effects arising from the interaction of incoming and outgoing pions with the target, as well as to include interactions of the struck nucleon with the residual core in both the initial and final states.

The single-nucleon bound-state wave function in the ground state was obtained from a parametrization of the Paris N-N potential [43] for ^{2}H, from an Eckart [44] form for ^{3}He, and using the parameterization of Greben [45] for ^{4}He.

The pion distorted waves were obtained from a modified Klein-Gordon equation [46] with a Kisslinger-type [47] optical potential together with kinematic "angle transformation" [48]. The optical potential parameters (b_0, b_1) for the incident channel were chosen such that the calculations reproduced our measured elastic-scattering angular distributions and the total reaction cross sections listed in Table II. (In the case of π^+-^{2}H scattering, the calculation was not able to reproduce the elastic cross sections when the kinematic "angle transformation" was included, and so it was not used.) Lacking a definite prescription for the energy dependence of the parameters (b_0, b_1), pions in the outgoing channel were distorted at the same energy (96.5 MeV) as the incident pions. The value of the parameters are listed in Table VI. Figure 4 shows the elastic differential cross sections for the three targets together with the optical model calculations.

The distorted waves for the knocked-out nucleon

TABLE VI. Optical model parameters (fm^3).

Target	Re(b_0)	Im(b_0)	Re(b_1)	Im(b_1)
^{2}H	−2.85	−1.15	14.74	0.91
π^+-^{3}He	−2.40	0.49	10.56	0.52
π^--^{3}He	−2.45	1.65	8.73	0.15
^{4}He	−0.67	0.44	7.88	0.69

were generated using a Woods-Saxon potential in a Schrödinger equation modified for relativistic effects [49]. The parameters of the Woods-Saxon well for ^{2}H was taken from the Reid soft-core N-N potential [50]. For ^{3}He and ^{4}He the parameters were obtained from an analysis [51, 52] of p-^{2}H and p-^{3}He forward-angle elastic-scattering data over an energy region of 20 to 100 MeV.

The measured and calculated (π, π') spectra are shown in Fig. 3, and the corresponding inelastic angular distributions are shown as curves in Fig. 6. There was no arbitrary normalization applied to the calculations in order to compare them to our data. Finally, the integrated inclusive single-charge-exchange cross sections were calculated using the DWIA. In Table VII we compare these calculated cross sections with the measured or estimated values presented in the previous section.

On the basis of the degree of agreement between the data and the calculated spectral shapes and cross-section magnitudes using the factorized DWIA, we judge that this model provides a good description of continuum inelastic scattering of pions from ^{2}H, ^{3}He, and ^{4}He at energies below the Δ resonance. Since the calculated (π, π') spectra and the cross sections are only the "quasifree" part of the total reaction cross section, the agreement supports the view that the bulk of the inelastic scattering proceeds through quasielastic scattering from a single nucleon. The DWIA result that π^+ and π^- on ^{3}He have nearly equal absorption cross sections follows from our general picture about the interplay of scattering and absorption. Distortion effects are found to be significant even for a few-nucleon system, such as ^{4}He. By comparison with PWIA and classical model calculations, we see that the main distortion effect appears to be pion absorption. The inelastic angular distributions for ^{2}H, ^{3}He, and ^{4}He are also well reproduced by in the DWIA, but the magnitudes of the calculated forward-angle (40°) cross sections are too large compared with our data for all of the targets.

V. SUMMARY AND CONCLUSIONS

We have measured the elastic and inclusive inelastic scattering of 96.5-MeV π^+ from ^{2}H, ^{3}He, and ^{4}He over a range of angles from 40° to 125° and of π^- from the helium isotopes over the range 60° to 125°. The inclusive inelastic scattering measurements cover an energy range for the scattered pion from about 25 MeV up to the maximum kinematically allowed energy. By using a high-pressure gas target and normalizing the measurements to scattering from ^{1}H, relative cross sections with accuracies of a few percent have been obtained for the π^+ measurements. From the π^- measurements on ^{3}He, we infer results for π^+ inelastic scattering from ^{3}H. We then discuss π^+ scattering from the four targets.

To interpret the results of our scattering measurements, we found it useful to combine our results with others from the available literature in order to estimate the true pion absorption cross sections which prevail in our targets at 96.5 MeV. The various pion cross sections are found to be consistent in character and magnitude with the assumption that pions scatter quasielastically from a single nucleon in the nucleus. The spectral shapes of the scattered pions are also in accord with this picture and so is the fact that the angular distributions of the inclusive inelastic scattering from the different targets resemble one another and also resemble (except for forward angles) the distribution for π^+ elastic scattering from ^{1}H at the same energy.

In order to understand these results in more detail, we carried out three different calculations based on a quasifree scattering picture. Complicating the comparison of the observed scattering to that from a free nucleon, there are effects from nucleon motion, true pion absorption, nuclear elastic scattering, and blocking. Each of the three calculations deals with (or ignores) these effects in various ways. We use a classical calculation to treat the competition between absorption and scattering. A modified PWIA calculation, which makes use of the result of the classical calculation, is used to separate elastic from inclusive inelastic scattering. Finally, DWIA

TABLE VII. Comparison of calculated and measured cross sections (mb).

	Inelastic		SCX		Absorption		Total reaction	
	Data	DWIA	Estimate[a]	DWIA	Data	Calc[b]	Data	Calc[c]
π^+-^{2}H	34.1±1.7	34.0	9.1±1.4	9.6	9.6± 0.2	9.9	53±3	53.5
π^+-^{3}He	67.3±3.2	68.7	9.5±1.4	10.1	20 ± 4	20.8	97±6	99.6
π^--^{3}He	32.0±4.3	40.0	15.5±3.1	20.8		22.9		83.7
π^+-^{4}He	42.1±1.5	40.5	11.3±1.7	11.8	63 ±10	55.3	116±9	107.6

[a] SCX estimate is based on measured inelastic cross section and isospin considerations, as discussed in the text.

[b] Calculated absorption is the difference of optical model total-reaction and DWIA cross sections.

[c] From optical model calculation.

calculations of the inclusive inelastic-scattering double-differential cross sections were done to study the consistency of the total reaction cross section with the elastic and inelastic ones.

In the classical picture, we assume that true absorption as well as scattering are both initiated by an interaction of the pion with a single nucleon. We match the measured absorption cross sections to a folding of the free pion-nucleon elastic cross section, mutual shadowing, and an assumed branching ratio for the initial complex leading to absorption rather than to scattering. We then examine whether these deduced branching ratios can be consistently understood for the different target nuclei in terms of their densities and the assumption that pion absorption occurs only on $T = 0$ nucleon pairs. We find reasonable consistency for mass 2 and mass 3, but the relatively large ratio of absorption to inelastic scattering for ^{4}He may reflect either an unusually large value of the absorption width or a relatively small value of the decay width. A relatively small decay width is expected for ^{4}He because of its large binding energy and the absence of bound states. An abnormally large absorption width in ^{4}He might arise from its unusually high density if multinucleon absorption can be considered a separate channel, not included in our model. We have not tried to make quantitative estimates of either of these effects.

We find that a simple PWIA calculation predicts angular distributions for inclusive inelastic scattering that have shapes similar to the measured ones, but the magnitude of the cross section is too large, as expected when the elementary interaction is strong. We correct the PWIA by including the attenuation of pion flux at the individual nucleons due to earlier pion interactions in the nucleus and also by including the branching between true absorption and scattering. These corrections produce angular distributions of similar shape to the simple calculations, but, except for ^{2}H, the magnitudes are now smaller than the measured differential cross sections. The decreasing inclusive inelastic differential cross sections at the most forward angles, common to the PWIA and the measurement, result from removal of flux from inelastic channels by the quasifree contribution to nuclear elastic scattering.

The DWIA calculation uses optical model parameters which are obtained by fitting the elastic differential cross sections and the total reaction cross sections to the experimentally determined values. With these parameters, the calculation reproduces the shapes of the inclusive inelastic spectra well. It also reproduces the magnitudes of the differential cross sections well at most angles, but it indicates that the inclusive inelastic angular distribution rises at forward angles, whereas the data do not exhibit this rise. We do not understand why the DWIA fails to reproduce the forward suppression so clearly seen in the PWIA.

Everything considered, most features of the inclusive inelastic scattering of 96.5-MeV pions by the nuclei with masses from 2 to 4 can be understood reasonably well in terms of a single encounter of the pion with a nucleon, in competition with true absorption.

The degree of quantitative success of the picture we have described for the interaction of pions just below the Δ resonance with both light and heavy nuclei benefits from the rapid fall off of pion cross section with decreasing pion energy along with the fact that in this energy regime quasielastic scattering tends to be backward with substantial energy loss. The pion, below the resonance, therefore remains an attractive projectile for the study of the possible modifications of projectile-nucleon interactions that occur inside nuclei. As the data improve and analyses of the type attempted here are refined, it may become possible to study some of these many-body effects with reasonable precision.

ACKNOWLEDGMENTS

We would like to express our thanks to the staff at TRIUMF for their support, especially to D.R. Gill for help with the M-11 channel and the QQD, to R. Openshaw for help with the wire chambers, and to K.A. Aniol for help with the gas compressor. Thanks are due J.F. Amann, D.D. Leach, D.H. Dowell, and S. Gil who helped with the data taking at various times. Finally, we would like to thank G.A. Miller, N.S. Chant, and P.G. Roos for many fruitful discussions about the DWIA calculations. This work was supported in part by the Department of Energy, and one of us (M.A.K.) was supported in part, while at the University of Maryland, by the NSF.

* Present address: Dept. of Physics and Astronomy, University of Maryland, College Park, MD 20742.

† Present address: Accelerator Laboratory, University of Saskatchewan, Saskatoon, SK, S7N 0W0 Canada.

‡ Present address: Department of Physics, Kyoto University, Kyoto 606, Japan.

§ Present address: Bates Linear Accelerator Center, Massachusetts Institute of Technology, P.O. Box 846 / 21 Manning Road, Middleton, MA 01949.

** Present address: Paul Scherrer Institute, CH-5234 Villigen PSI, Switzerland.

[1] M. Baumgartner H. P. Gubler, G. R. Plattner, W. D. Ramsay, H. W. Roser, I. Sick, P. Zupranski, J. P. Egger, and M. Thies, Nucl. Phys. **A399**, 451 (1983).

[2] C. H. Q. Ingram, P. A. M. Gram, J. Jansen, R. E. Mischke, J. Zichy, J. Bolger, E. T. Boschitz, G. Pröbstle, and J. Arvieux, Phys. Rev. C **27**, 1578 (1983).

[3] A. Klein, C. Gysin, R. Henneck, J. Jourdan, M. Pickar, G. R. Plattner, I. Sick, and J. P. Egger, Nucl. Phys. **A472**, 605 (1987).

[4] S. M. Levenson, D. F. Geesaman, E. P. Colton, R. J. Holt, H. E. Jackson, J. P. Schiffer, J. R. Specht, K. E. Stephenson, B. Zeidman, R. E. Segel, P. A. M. Gram, and C. A. Goulding, Phys. Rev. C **28**, 326 (1983).

[5] R. D. McKeown, S. J. Sanders, J. P. Schiffer, H. E. Jackson, M. Paul, J. R. Specht, E. J. Stephenson, R. P. Redwine, and R. E. Segel, Phys. Rev. C **24**, 211 (1981).

[6] K. A. Aniol, D. T. Chiang, K. G. R. Doss, I. Halpern, M. A. Khandaker, D. W. Storm, D. R. Tieger, P. D. Barnes, B. Bassalleck, N. J. Colella, S. A. Dytman, R.

A. Eisenstein, R. Grace, C. Maher, D. Marlow, P. Pile, R. Rieder, F. Takeutchi, W. R. Wharton, J. F. Amann, and J. Julien, Phys. Rev. C **33**, 208 (1986).
[7] P. A. M. Gram, S. A. Wood, E. R. Kinney, S. Høibråten, P. Mansky, J. L. Matthews, T. Soos, G. A. Rebka, Jr., and D. A. Roberts, Phys. Rev. Lett. **62**, 1837 (1989).
[8] R. Mach, M. G. Sapozhnikov, and I. V. Falomkin, Fiz. Elem. Chastis At. Yadra **17**, 1231 (1986) [Sov. J. Part. Nucl. **17**, 549 (1986)].
[9] D. Ashery, R. J. Holt, H. E. Jackson, J. P. Schiffer, J. R. Specht, K. E. Stephenson, R. D. McKeown, J. Ungar, R. E. Segel, and P. Zupranski, Phys. Rev. Lett. **47**, 895 (1981).
[10] J. Källne, R. C. Minehart, R. R. Whitney, R. L. Boudrie, J. B. McClelland, and A. W. Stetz, Phys. Rev. C **28**, 304 (1983).
[11] M. A. Moinester, D. R. Gill, J. Vincent, D. Ashery, S. Levenson, J. Alster, A. Altman, J. Lichtenstadt, E. Piasetzky, K. A. Aniol, R. R. Johnson, H. W. Roser, R. Tacik, W. Gyles, B. Barnett, R. J. Sobie, and H. P. Gubler, Phys. Rev. Lett. **52**, 1203 (1984), including the correction factor of 0.83 discussed in Ref. 12.
[12] K. A. Aniol, A. Altman, R. R. Johnson, H. W. Roser, R. Tacik, U. Wienands, D. Ashery, J. Alster, M. A. Moinester, E. Piasetzky, D. R. Gill, and J. Vincent, Phys. Rev. C **33**, 1714 (1986).
[13] G. Backenstoss, M. Izycki, P. Salvisberg, M. Steinacher, P. Weber, H. -J. Weyer, S. Cierjacks, S. Ljungfelt, H. Ullrich, M. Furić, and T. Petković, Phys. Rev. Lett. **55**, 2782 (1985).
[14] D. Ashery and J. P. Schiffer, Annu. Rev. Nucl. Part. Sci. **36**, 207 (1986) and references therein.
[15] G. Backenstoss, M. Izycki, P. Salvisberg, M. Steinacher, P. Weber, H.-J. Weyer, S. Cierjacks, B. Rzehorz, H. Ullrich, M. Furić, T. Petković, and N. Simićević, Phys. Rev. Lett. **59**, 767 (1987).
[16] G. Backenstoss, D. Brodbeck, M. Izycki, P. Salvisberg, M. Steinacher, P. Weber, H. -J. Weyer, A. Hoffart, B. Rzehorz, H. Ullrich, D. Bosnar, M. Furić, and T. Petković, Phys. Rev. Lett. **61**, 923 (1988).
[17] B. G. Ritchie, G. S. Blanpied, R. S. Moore, B. M. Preedom, K. Gotow, R. C. Minehart, J. Boswell, G. Das, H. J. Ziock, N. S. Chant, P. G. Roos, W. J. Burger, S. Gilad, and R. P. Redwine, Phys. Rev. C **27**, 1685 (1983).
[18] G. M. Stinson, TRIUMF Internal Report TRI-DNA-80-5, 1980 (unpublished).
[19] K. A. Aniol, R. Tacik, W. Gyles, R. R. Johnson, D. F. Ottewell, D. R. Gill, and G. M. Stinson, TRIUMF Internal Report TRI-DN-81-12, 1981 (unpublished).
[20] D. R. Gill, S. Martin, and R. J. Sobie, TRIUMF Internal Report TRI-DN-81-10, 1981 (unpublished).
[21] R. J. Sobie, T. E. Drake, B. M. Barnett, K. L. Erdman, W. Gyles, R. R. Johnson, H. W. Roser, R. Tacik, E. W. Blackmore, D. R. Gill, S. Martin, C. A. Wiedner, and T. Masterson, Nucl. Instrum. Methods **219**, 501 (1984).
[22] M. A. Khandaker, Ph.D. thesis, University of Washington, 1987 (unpublished).
[23] G. Rowe, M. Salomon, and R. H. Landau, Phys. Rev. C **18**, 584 (1978).
[24] J. Källne, J. F. Davis, J. S. McCarthy, R. C. Minehart, R. R. Whitney, R. L. Boudrie, J. B. McClelland, and A. W. Stetz, Phys. Lett. **103B**, 13 (1981).
[25] E. G. Pewitt, T. H. Fields, G. B. Yodh, J. G. Fetkovich, and M. Derrick, Phys. Rev. **131**, 1826 (1963).
[26] T. J. Bowles, D. F. Geesaman, R. J. Holt, H. E. Jackson, J. Julien, R. M. Laszewski, J. R. Specht, E. J. Stephenson, R. P. Redwine, L. L. Rutledge, R. E. Segel, and M. A. Yates, Phys. Rev. C **23**, 439 (1981).
[27] E. R. Kinney, Ph.D. thesis, MIT, 1988 (unpublished).
[28] E. R. Kinney, J. L. Matthews, P. A. M. Gram, D. W. MacArthur, E. Piasetzky, G. A. Rebka, Jr., and D. A. Roberts, Phys. Rev. Lett. **57**, 3152 (1986).
[29] F. Balestra, M. P. Bussa, L. Busso, R. Garfagnini, G. Piragino, C. Guaraldo, A. Maggiora, R. Scrimaglio, I. V. Falomkin, G. B. Pontecorvo, and Yu. A. Shcherbakov, Nucl. Phys. **A340**, 372 (1980).
[30] F. Balestra, S. Bossolasco, M. P. Bussa, L. Busso, L. Ferrero, D. Panzieri, G. Piragino, F. Tosello, I. V. Falomkin, V. I. Lyashenko, G. B. Pontecorvo, Yu. A. Shcherbakov, D. Cauz, R. Garfagnini, L. Shanti, and A. Maggiora, Il Nuovo Cimento **92A**, 139 (1986).
[31] E. Bellotti, D. Cavalli, and C. Matteuzzi, Il Nuovo Cimento **18A**, 75 (1973).
[32] E. C. Fowler, W. B. Fowler, R. P. Shutt, A. M. Thorndike, and W. L. Whittemore, Phys. Rev. **91**, 135 (1953).
[33] K. F. Johnson, Ph.D. thesis, New Mexico State University, 1976 (unpublished).
[34] F. Binon, P. Duteil, M. Gouanére, L. Hugon, J. Jansen, J.-P. Lagnaux, H. Palevsky, J.-P. Peigneux, M. Spighel, and J.-P. Stroot, Nucl. Phys. **A298**, 499 (1978)
[35] Z. Fraenkel, E. Piasetzky, and G. Kolbermann, Phys. Rev. C **26**, 1618 (1982).
[36] J. N. Ginocchio and M. B. Johnson, Phys. Rev. C **21**, 1056 (1980).
[37] D. Rosenzweig, I. Halpern, M. Khandaker, D. W. Storm, J. Nelson, D. Tieger, S. Wood, K. Doss, J. Amann, R. Boudrie, and D. Drake, Bull. Am. Phys. Soc. **34**, 1204 (1989).
[38] T. K. Fowler and K. M. Watson, Nucl. Phys. **13**, 549 (1959)
[39] N. S. Chant and P. G. Roos, Phys. Rev. C **15**, 57 (1977).
[40] P. G. Roos, L. Rees, and N. S. Chant, Phys. Rev. C **24**, 2647 (1981).
[41] L. Rees, N. S. Chant, and P. G. Roos, Phys. Rev. C **26**, 1580 (1982).
[42] N. S. Chant, L. Rees, and P. G. Roos, Phys. Rev. Lett. **48**, 1784 (1982).
[43] M. Lacombe, B. Loiseau, R. Vinh Mau, J. Côté, P. Pirés, and R. de Tourreil, Phys. Lett. **101B**, 139 (1981).
[44] T. K. Lim, Phys. Lett. **43B**, 349 (1973).
[45] J. M. Greben, Phys. Lett. **115B**, 363 (1982).
[46] E. H. Auerbach, D. M. Fleming, and M. M. Sternheim, Phys. Rev. **162**, 1683 (1967).
[47] L. S. Kisslinger, Phys. Rev. **98**, 761 (1955).
[48] N. J. DiGiacomo, A. S. Rosenthal, E. Rost, and D. A. Sparrow, Phys. Lett. **66B**, 421 (1977).
[49] A. Nadasen, P. Schwandt, P. P. Singh, W. W. Jacobs, A. D. Bacher, P. T. Debevec, M. D. Kaitchuck, and J. T. Meek, Phys. Rev. C **23**, 1023 (1981).
[50] R. V. Reid, Ann. Phys. **50**, 411 (1968).
[51] J. S. Wesick, Ph.D. thesis, University of Maryland, 1983 (unpublished).
[52] B. S. Podmore and H. Sherif, in *Few Body Problems in Nuclear and Particle Physics*, Quebec, 1975, edited by R. J. Slobodrian, B. Cujec, and K. Ramavataram (Univ. of Laval Presses, Quebec, 1975), p. 517.